RESEARCH ARTICLE

Photovoltaics and photoelectrochemistry

Energy & Environmental Materials WILEY

A Comprehensive Analysis of Recombination at Grain Boundaries in High-Efficiency Kesterite-Type Solar Cells

*Daniel Abou-Ras**, *Sebastian Weitz*, *Jialiang Huang*, *Kaiwen Sun*, *Yuancai Gong*, *Alex Jimenez-Arguijo*, *Mirjana Dimitrievska*, *Xiaojing Hao*, *and Edgardo Saucedo*

The present work reports on microscopic analyses of recombination at grain boundaries (GBs) in polycrystalline Li-doped $(Ag,Cu)_2ZnSn(S,Se)_4$ (Li-ACZTSSe) and Cu_2ZnSnS_4 (CZTS) absorber layers in high-efficiency solar cells (conversion efficiencies of 14.4% and 10.8%). Recombination velocities s_{GB} were determined at a large number of GBs by evaluating profiles extracted from cathodoluminescence intensity distributions across GBs in these polycrystalline layers. In both Li-ACZTSSe and CZTS absorber layers, the s_{GB} values exhibited wide ranges over several orders of magnitude with a median values of 680 and 1100 cm s^{-1} for the Li-ACZTSSe and CZTS absorbers. A model that provides a comprehensive explanation for this finding is presented and discussed in detail. Correspondingly, wide ranges for s_{GB} can be explained by different positive or negative excess charge densities present at different GBs, leading to different downward or upward band bending on the order of several $\pm$10 meV, provided that the net-doping density of the absorber layers is sufficiently large. As a result of the evaluation of the s_{GB}, input parameters for multidimensional device simulations are obtained. It is revealed that the grain boundary lifetime closely matches the overall effective lifetime, indicating that grain boundary recombination is a key factor limiting the effective carrier lifetime of both Li-ACZTSSe and CZTS absorbers. The estimated V_{OC} losses due to GBs reach up to 126 mV for Li-ACZTSSe and 88 mV for CZTS. This work highlights that reducing grain boundary recombination via improved passivation and increasing grain size is an effective strategy for achieving further efficiency improvements.

1. Introduction

Kesterite-type materials such as copper–zinc–tin–sulfide (Cu_2ZnSnS_4, CZTS) and copper–zinc–tin–selenide ($Cu_2ZnSnSe_4$, CZTSe) have attracted significant attention as promising candidates for low-cost, environmentally friendly solar cells.[1,2] Composed of earth-abundant, low-toxicity elements, these materials offer a sustainable alternative to conventional thin-film photovoltaic technologies such as $Cu(In,Ga)Se_2$ (CIGS) and CdTe. With tunable bandgaps of ~1.0–1.5 eV and high absorption coefficients ($>10^4$ cm^{-1}), kesterite-type absorbers are well-suited for solar energy conversion. In recent years, substantial advancements in synthesis methods, post-deposition treatment, and doping/alloying strategies have advanced the technology of kesterite-type solar cells. Encouragingly, the power conversion efficiency (PCE) of $(Ag,Cu)_2ZnSn(S,Se)_4$ (ACZTSSe) solar cells is surpassing 15%, and widegap Cu_2ZnSnS_4 (CZTS) solar cells have surpassed the efficiency level of 13%, marking an important step toward the advancement of sustainable, earth-abundant thin-film photovoltaics.[3–9]

Further closing the gap that remains between current efficiencies and the theoretical Shockley-Queisser limit to achieve efficiencies of beyond 20% will require overcoming several critical challenges. The most pressing one is reducing the non-radiative recombination losses, as current-state-of-the-art open-circuit voltage (V_{OC}) deficits of 300–350 mV impede further improvements of the solar cells performance.[2,9–11] One origin of Voc losses in kesterite-type solar cells is nonradiative Shockley–Read–Hall recombination at grain boundaries (GBs). Ab initio calculations demonstrated that strong cation–cation (e.g. Cu–Sn) and anion-anion (S–S) bonds at GBs can introduce mid-gap states, acting as recombination centers.[12,13]

Dr. D. Abou-Ras, S. Weitz
Department for Structure and Dynamics of Energy Materials, Helmholtz-Zentrum Berlin für Materialien und Energie GmbH, Hahn-Meitner-Platz 1, Berlin 14109, Germany
E-mail: daniel.abou-ras@helmholtz-berlin.de
Dr. J. Huang, Dr. K. Sun, Prof. X. Hao
Australian Centre for Advanced Photovoltaics, School of Photovoltaic and Renewable Energy Engineering, University of New South Wales, Sydney, NSW 2052, Australia
Dr. Y. Gong, Dr. A. Jimenez-Arguijo, Prof. E. Saucedo
Electronic Engineering Department, Universitat Politècnica de Catalunya (UPC), Photovoltaic Lab — Micro and Nano Technologies Group (MNT), EEBE, Av Eduard Maristany 10-14, Barcelona 08019, Catalonia, Spain
Barcelona Center for Multiscale Science & Engineering, Universitat Politècnica de Catalunya (UPC), Av Eduard Maristany 10-14, Barcelona 08019, Catalonia, Spain
Dr. M. Dimitrievska
Transport at Nanoscale Interfaces Laboratory, Swiss Federal Laboratories for Material Science and Technology (EMPA), Ueberlandstrasse 129, CH-8600, Duebendorf, Switzerland
The ORCID identification number(s) for the author(s) of this article can be found under https://doi.org/10.1002/eem2.70048.

DOI: 10.1002/eem2.70048

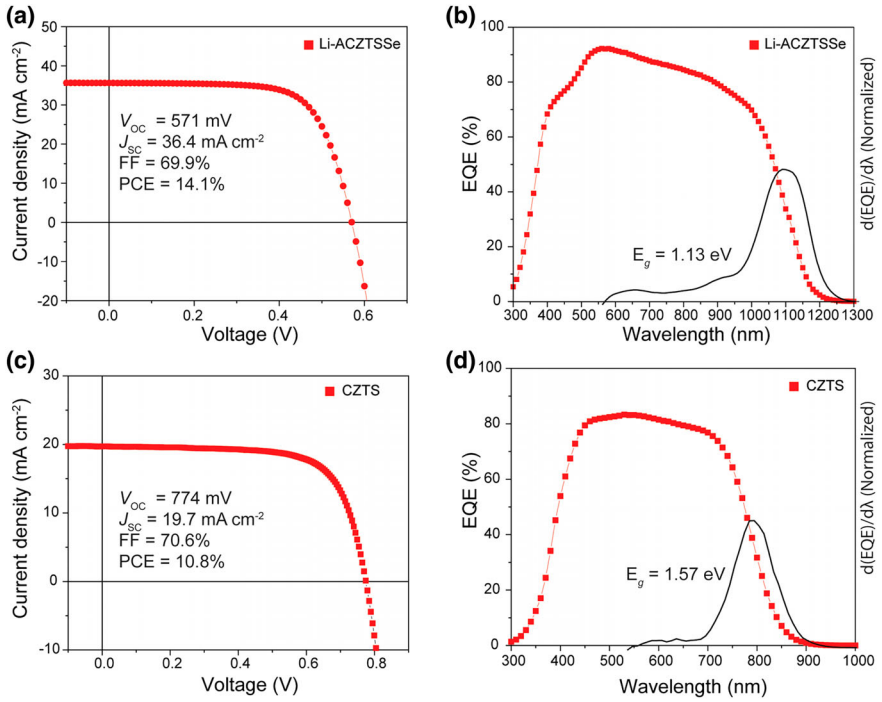

Figure 1. *J–V* and EQE curves of a, b) Li-ACZTSSe ($E_g = 1.13$ eV) and c, d) CZTS ($E_g = 1.57$ eV) devices. Bandgap of the absorber estimated from first derivatives of EQE.

However, defect segregation mechanisms have been proposed, showing that Zn-rich (Cu-poor) terminations minimize surface energy, act as hole reflectors, and reduce the density of mid-gap states.[12–14] Additionally, the volatility of chalcogens can lead to chalcogen vacancies at the GBs, which might be passivated through the incorporation of alkali metals and oxygen incorporation.[13–15] However, investigations on the recombination properties of GBs in kesterites remain scarce,[12,16–19] and most publications reporting experimental improvements attributed to reduced GB recombination rely solely on contact potential difference (CPD) distributions obtained from Kelvin probe force microscopy (KPFM) measurements.[11,15,20–29] To date, Li et al.[30] is the only study directly analyzing recombination velocities at GBs (s_{GB}) in kesterite-type absorber layers, indicating high nonradiative recombination; however, its statistical significance is limited due to the small number of GBs investigated.

In the present work, we examined systematically a large number of GBs in high-efficiency Li-doped $(Ag,Cu)_2ZnSn(S,Se)_4$ (Li-ACZTSSe) and Cu_2ZnSnS_4 (CZTS) solar cells with PCEs of 14.4% and 10.8%, using electron backscatter diffraction (EBSD) and cathodoluminescence (CL) in scanning electron microscopy (SEM) to assess the positions of the GBs and the recombination velocities at GBs s_{GB}, as well as time-resolved photoluminescence (TRPL) to determine the effective lifetimes in the absorber layers. The s_{GB} values obtained at different GBs in both absorber layers exhibited ranges over several orders of magnitude. Numerical simulations indicate that the corresponding downward and upward band bending at GBs varies on the order of several ±10 meV, which may be attributed to the presence of different positive or negative excess charges at individual GBs. Grain boundary recombination was found to be a key factor limiting the effective carrier lifetime in both Li-ACZTSSe and CZTS absorbers, with estimated V_{OC} losses reaching up to 126 mV for Li-ACZTSSe and 88 mV for CZTS. This work highlights that reducing grain boundary recombination through improved passivation and increased grain size offers a promising pathway for further efficiency improvements.

2. Results and Discussion

The high-efficiency Li-ACZTSSe device exhibits a V_{OC} of 571 mV, a short-circuit current (J_{SC}) of 36.4 mA cm^{-2}, and a fill factor (FF) of 69.9%, resulting in a PCE of 14.4% (see **Figure 1a** for the corresponding *j-V* curves). These photovoltaic parameters are among the best reported for ACZTSSe solar cells to date, making its absorber an excellent candidate for studying the intrinsic properties of GBs. The capacitance–voltage measurements showed that the net-doping concentration in this absorber was 2×10^{16} cm^{-3}.[9] This moderately high carrier concentration is consistent with optimal doping levels for CZTSSe-based solar cells.[31,32] Additionally, time resolved photoluminescence spectroscopy (TRPL) measurements conducted on the Li-ACZTSSe/Mo/glass stack reveal an effective minority-carrier lifetime of ~16 ns (Figure S1, Supporting Information). The activation energy (E_a) of the ACZTSSe/CdS interface, extracted from the temperature-dependent j-*V* measurements, is 1.13 eV, matching the absorber's bandgap (E_g), as shown in Figure 1b and Figure S2, Supporting Information. This indicates that interface recombination is not the dominant recombination mechanism. Instead, recombination primarily occurs within the absorber bulk, including grain interiors and boundaries, making it an ideal platform for studying grain boundary properties and V_{OC} loss mechanisms of the kesterite devices. On the other hand, the j-*V* analysis of the CZTS solar cell (Figure 1c) revealed a V_{OC} of 774 mV, a J_{SC} of 19.7 mA cm^{-2}, a fill factor (FF) of 70.6%, and a PCE of 10.8%. The bandgap of the CZTS device is 1.57 eV, determined by EQE, shown in Figure 1d. The net-doping density was determined to be 1×10^{16} cm^{-3} by CV measurement (Figure S4a, Supporting Information). The effective minority-carrier lifetime measured by TRPL on the CZTS device was about 4 ns (Figure S4b, Supporting Information).

Microscopic analyses were performed on cross-sectional specimens of the Li-ACZTSSe and CZTS solar-cell stacks. Elemental distribution maps from these solar-cell stacks acquired by means of energy-dispersive X-ray spectroscopy (EDXS) are given in Figure S5, Supporting Information. Zn(S,Se) and ZnS secondary phases were detected in the Li-ACZTSSe and CZTS absorber layers.

From the electron backscatter diffraction (EBSD) maps (**Figures 2** and **3**), the average grain sizes (diameters of circles that exhibit the same areas as the grains) were estimated to be about 0.7 and 0.3 μm for the Li-ACZTSSe and CZTS thin films (see Figure S6, Supporting Information for the corresponding grain-size distributions). The value for the Li-ACZTSSe layer is consistent with the findings from the top-view image shown in Figure S3, Supporting Information. Both absorber layers do not exhibit any substantial film texture. In the CL intensity distributions (Figures 2d and 3d), the CL signals are reduced

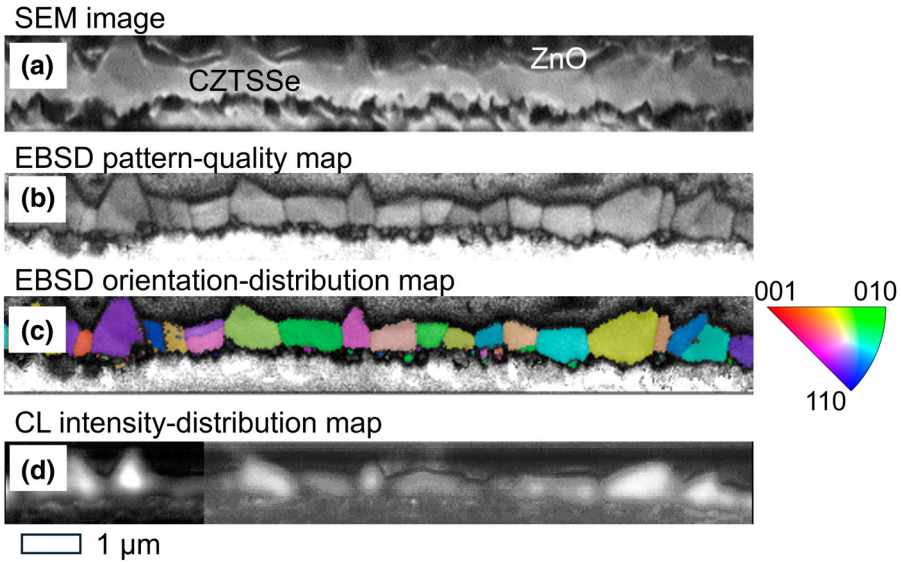

Figure 2. a) SEM image b) EBSD pattern-quality and c) orientation–distribution maps, with the local orientations perpendicular to the substrate given as false colors (see legend), as well as d) CL intensity distributions, all acquired on the identical area of a cross-sectional specimen of the Li-ACZTSSe solar cell.

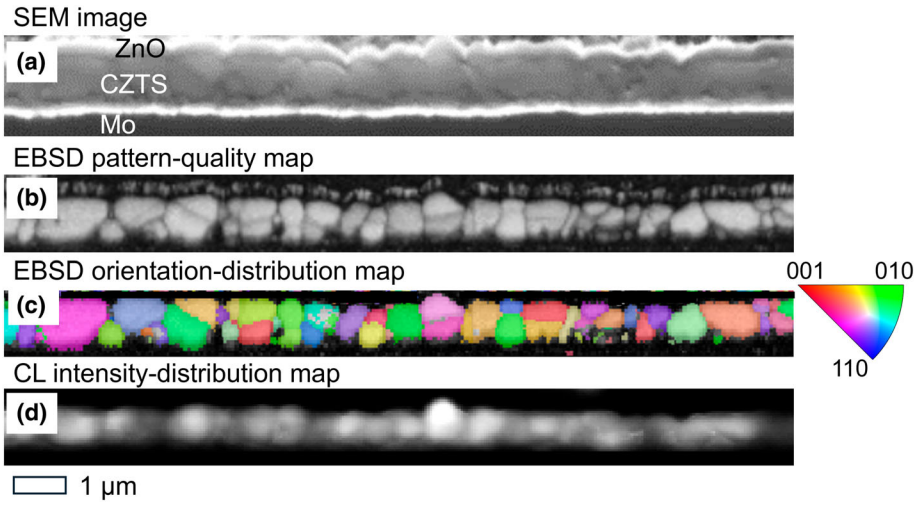

Figure 3. a) SEM image b) EBSD pattern-quality and c) orientation–distribution maps, with the local orientations perpendicular to the substrate given as false colors (see legend), as well as d) CL intensity distributions, all acquired on the identical area of a cross-sectional specimen of the CZTS solar cell.

at randomly oriented GBs, while twin boundaries did not exhibit any change in the CL intensity (verified by the EBSD maps).

Through a combined analysis of CL linescan profiles, grain size distributions from EBSD, and effective lifetimes (?$_{???}$) obtained from TRPL, the grain boundary recombination velocity (s_{GB}) and minority carrier lifetime at the grain boundary (τ_{GB}) can be determined, using the approach described in Refs.[33,34] (outlined in the SI). The resulting recombination velocities determined at the various GBs in the Li-ACZTSSe and CZTS absorbers are given in **Figure 4**a,b. Apparently, their values range over several orders of magnitude for both absorber layers: about 10^0–10^4 and 10^2–10^4 cm s^{-1} for Li-ACZTSSe and CZTS.

This behavior of the s_{GB} values can be understood by using the following expression, which is valid for p-type semiconductors and for low-injection conditions[35]

$$s_{GB} = s^n_{GB,0} \exp\left(-\Phi_{GB}\left(N_{GB,charge}\right)/k_B T\right). \quad (1)$$

Here, $N_{GB,charge}$, Φ_{GB}, k_B, and T are the effective, excess charge density at the grain boundary, the upward or downward band bending at the grain boundary (due to redistribution of free charge carriers), the Boltzmann constant, and the absolute temperature. The prefactor $s^n_{GB,0}$ is the product of the effective defect density at a GB, of its capture cross-section for electrons, and of the thermal velocity of electrons (see Mendis et al.[35] for further details) and describes the enhanced, nonradiative Shockley–-Read–Hall recombination at the GB plane. Note that a prerequisite for the application of Equation (1) is that Φ_{GB} exhibits an upper/lower limit of about ±100 meV.[35] This upward and downward band bending in Equation (1) can be expressed by[35]

$$\Phi^{up}_{GB} = \left(k_B T\right)^{0.5} e N_{GB,charge} / \left[4\left(\varepsilon_0 \varepsilon_r N_A\right)^{0.5}\right] \quad (2)$$

and[36]

$$\Phi^{down}_{GB} = -e^2 N^2_{GB,charge} / \left(8 \varepsilon_0 \varepsilon_r N_A\right). \quad (3)$$

where ε_0 and ε_r are the dielectric permittivity of the vacuum and of the thin-film material. Note that for given T, ε_r and N_A, Φ^{up}_{GB} and Φ^{down}_{GB} are functions only of $N_{GB,charge}$, that is, s_{GB} is a function of $N_{GB,charge}$ and $s^n_{GB,0}$. We can now determine the ranges for $N_{GB,charge}$ and $s^n_{GB,0}$ for which Equation (13) simulate successfully the s_{GB} values in Figure 4. For this step, we assumed that in the Li-ACZTSSe and CZTS thin films, the interdiffusion of point defects during the film growth at elevated temperatures leads to a quasi-homogeneous distribution of the $N_{GB,charge}$ at the GBs, that is, the magnitudes of $N_{GB,charge}$ remain within about the same order of magnitude for all GBs in the same layer. Since it can be expected that the ensemble of point defects at GBs and therefore, the excess-charge density $N_{GB,charge}$ (and Φ_{GB} via Equations 2 and 3) is different (positive or negative) at different GBs, and since these point defects, as an ensemble, exhibit different enhanced, nonradiative recombination expressed by different $s^n_{GB,0}$ values for different GBs, the result is different recombination velocities via Equation 1.

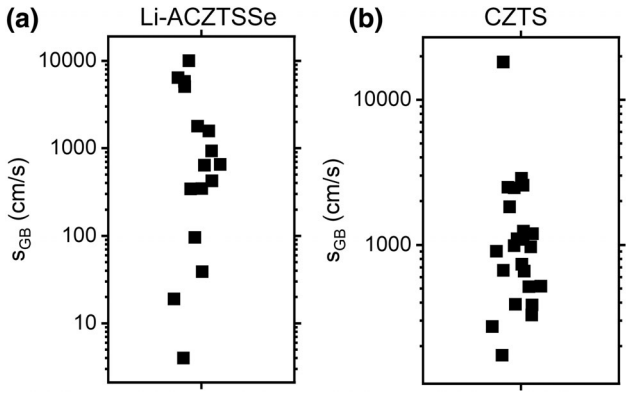

Figure 4. Recombination velocities s_{GB} determined on a) the Li-ACZTSSe and b) the CZTS absorber layers. The symbols are distributed in a horizontal direction to avoid strong overlaps of the symbols.

Concerning $s^{n}_{GB,0}$, we set their ranges such that they are on the same order of magnitude as the median of the s_{GB} values (about 680 and 1100 cm s^{-1} for the Li-ACZTSSe and CZTS absorbers). The corresponding results are shown in **Figures 5** and **6**. Apparently, $N_{GB,charge}$ and $s^{n}_{GB,0}$ ranges that are used to simulate successfully the experimental s_{GB} values are about $0.9–9 \times 10^{11}$ cm^{-2} and $0.2–2 \times 10^{-16}$ cm^{2} as well as 100–1000 and 500–2000 cm s^{-1} for the Li-ACZTSSe and CZTS absorbers. The band bending in both downward and upward directions remains within the interval of ±100 meV. It is well visible in Figures 5 and 6 that some s_{GB} values can be simulated assuming only downward or only upward band bending, while others can be modeled considering both downward and upward band bending.

We note that the magnitudes of the $N_{GB,charge}$ and $s^{n}_{GB,0}$ ranges depicted in Figures 5 and 6 are in good agreement with results obtained on GBs in those ACIGSe and mc-Si solar absorbers, which also exhibit net-doping densities of about 10^{16} cm^{-3} as the kesterite-type absorbers in the present work.[35] Thus, we can conclude that the GB properties leading to the measured recombination velocities are similar in the different absorber materials. However, the GB lifetime for kesterite-type absorbers should be substantially smaller due to the smaller average grain size compared with that in materials such as mc-Si, according to Equation S3, Supporting Information. This Equation S3, Supporting Information, highlights also that the GB lifetime in the absorber layers and therefore, the device performance of corresponding solar cells, can be improved by increasing the average grain size and passivation of GB (i.e., decreasing the median GB recombination velocity).

The results in Figures 5 and 6 indicate different positive or negative excess charges at different GBs, leading to different upward or downward band bending on the order of several ±10 meV. Because of these small band bending values, the transport of charge carriers across GB planes and therefore, the short-circuit current in corresponding solar cells is not affected considerably, as shown for GBs in Cu(In,Ga)Se$_2$ solar cells.[37] This is, the main impact of GBs on the device performance of solar cells is a decrease of the open-circuit voltage V_{OC} (and of the corresponding part of the fill factor) by enhanced nonradiative recombination at GBs. For multidimensional device simulations of CZTSSe-based solar cells, the estimates of the $N_{GB,charge}$ and $s^{n}_{GB,0}$ represent important input parameters (see, e.g., Krause et al.[37]); according to Equations (1–3), only they are needed to simulate any s_{GB} value for a given net-doping density and absolute temperature.

As outlined in the SI, the median s_{GB} values as well as the minority-charge carrier lifetimes in the bulk and at GBs (τ_{bulk}, τ_{GB}) were extracted. By iteratively applying diffusion length fitting (Equation S1, Supporting Information) and lifetime relations (Equations S2, S3, Supporting Information), s_{GB}, τ_{bulk}, and τ_{GB} were determined for each material, with median GB recombination velocities of 680 and 1100 cm s^{-1} in Li-ACZTSSe and CZTS. The corresponding lifetime values and the average grain sizes for the Li-ACZTSSe and CZTS layers are listed in Table S1, Supporting Information. It is apparent that for both layers, $\tau_{eff,material}$ and τ_{GB} are very close to one another, suggesting that the effective carrier lifetime is limited primarily by τ_{GB}.

The determined s_{GB} and lifetime values were further used to assess the contribution of grain boundary recombination to V_{OC} losses, accounting for both bulk and interface recombination effects (Equations S4–S7, Supporting Information). Figure S7, Supporting Information illustrates the estimated V_{OC} losses in the Li-ACZTSSe and CZTS, with τ_{interf} varying between the value of the τ_{bulk} and τ_{GB} (16–200 ns for Li-ACZTSSe and 5–20 ns for the CZTS sample). The case for cells with perfect contacts is also calculated as a separate point in the graph. It is shown that the V_{OC} losses can reach up to 126 mV and 88 mV for Li-ACZTSSe and CZTS, for an ideality

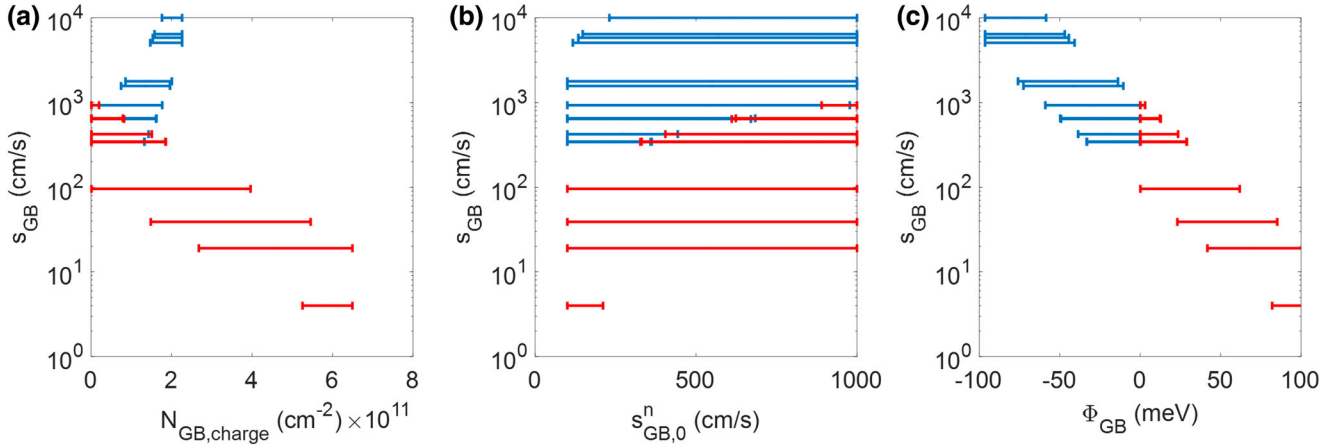

Figure 5. Experimental s_{GB} values for Li-ACZTSSe, simulated successfully using the ranges of a) $N_{GB,charge}$ and of b) $s^{n}_{GB,0}$ and resulting in the band bending value c) Φ_{GB}. The blue bars represent downward, and the red bars upward band bending.

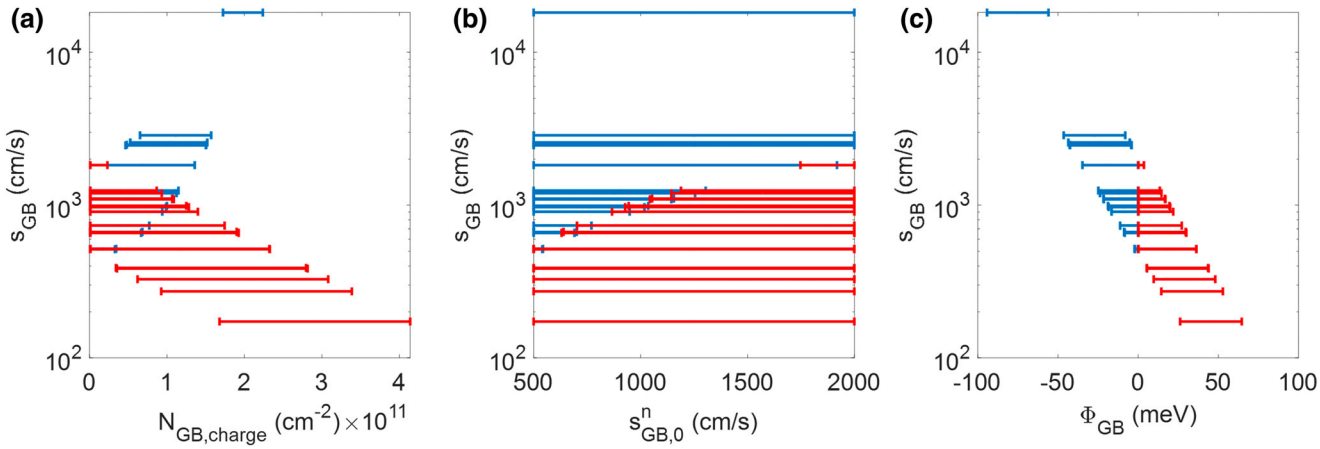

Figure 6. Experimental s_{GB} values for CZTS, simulated successfully using the ranges of a) $N_{GB,charge}$ and of b) $s^n_{GB,0}$, resulting in the band bending value c) Φ_{GB}. The blue bars represent downward, and the red bars upward band bending.

factor of $n_{id} = 1$. The estimated *VOC* losses increase with a larger ideality factor. While these gains do not fully explain the V_{OC} deficits of several 100 mV reported for CZTSSe devices, they highlight that GB recombination remains a significant bottleneck to improving τ_{eff} and, consequently, V_{OC}.

3. Conclusions

Recombination at GBs in Li-ACZTSSe and CZTS absorber layers, of which the solar cells exhibited PCEs of 14.1% and 10.7%, was analyzed in detail using microscopic characterization. In both absorber layers, the recombination velocities s_{GB} are distributed over several orders of magnitude, in good correspondence with s_{GB} values determined on GBs in wafer-based mc-Si as well as in polycrystalline ACIGSSe and CdTe thin films. These large ranges for s_{GB} can be explained by different positive or negative excess charge densities present at different GBs, leading to downward or upward band bending on the order of several ±10 meV. The extracted values for the excess charge density $N_{GB,charge}$ and for the prefactor $s^n_{GB,0}$ represent important input parameters for multidimensional device simulations. The grain boundary lifetimes corresponding to the median grain boundary recombination velocities were found to closely match the overall effective lifetime from TRPL measurement, indicating that grain boundary recombination is a key factor limiting the effective carrier lifetime of both Li-ACZTSSe and CZTS absorbers. The estimated V_{OC} losses due to GBs reach up to 126 mV for Li-ACZTSSe and 88 mV for CZTS. The present work highlights that reducing GB recombination via improved passivation (i.e., decreasing s_{GB}) and increased grain size is an effective strategy for achieving further efficiency improvements.

Acknowledgements

D.A. and S.W. are grateful for support by the German-Israeli Helmholtz International Research School HI-SCORE (HIRS-0008) and by the project "EFFCIS II" funded by the Federal Ministry for Economic Affairs and Climate Action (BMWK) under contract numbers 03EE1059B. This work received funding from the Australian Renewable Energy Agency (ARENA) as part of ARENA's Transformative Research Accelerating Commercialization (TRAC) Program, the Australian Research Council (ARC) Discovery Project (DP230102463), Linkage Project (LP200301593) and Baosteel-Australia Joint Research and Development Center (BA19010). K. S. acknowledges the Australian Research Council (ARC) Discovery Early Career Researcher Award (DE230100021) and support from the Australian Center of Advanced Photovoltaics (ACAP) as a recipient of the ACAP Fellowship (RG172864-B). X. H. acknowledges the financial support of the Australian Research Council (ARC) Future Fellowship (FT190100756). This project received funding from the European Union's H2020 ERC-Consolidator program under grant agreement number no. 866018 (SENSATE), and by the Science and Innovation Ministry of Spain projects number PID2023-148976OB-C41 (CURIO-CITY) and PCI2023-145971-2 (ACT-FAST, CET-Partnership 2023 program). Y.G. thanks the European Union's Horizon research and innovation program under the Marie Skłodowska-Curie grant agreement no. 10115148 (LEK-PV). The authors from UPC belong to the Micro and Nanotechnologies for Solar Energy Group (MNTSolar) Consolidated Research Group of the "Generalitat de Catalunya" (2021 SGR 01286). This work is also part of Maria de Maeztu Units of Excellence Program CEX2023-001300-M/funded by MICIU/AEI/10.13039/501100011033. E.S. is grateful to ICREA Academia program. Open Access funding enabled and organized by Projekt DEAL.

Conflict of Interest

The authors declare no conflict of interest.

Data Availability Statement

The data shown in the present work is available from the authors upon reasonable request.

Supporting Information

Supporting Information is available from the Wiley Online Library or from the author.

Keywords

cathodoluminescence, grain boundaries, kesterite, recombination velocity, solar cells

Received: March 21, 2025
Revised: April 28, 2025
Published online: May 12, 2025

[1] A. Wang, M. He, M. A. Green, K. Sun, X. Hao, *Adv. Energy Mater.* **2023**, *13*, 2203046.
[2] S. Giraldo, Z. Jehl, M. Placidi, V. Izquierdo-Roca, A. Pérez-Rodríguez, E. Saucedo, *Adv. Mater.* **2019**, *31*, 1806692.
[3] J. Shi, J. Wang, F. Meng, J. Zhou, X. Xu, K. Yin, L. Lou, M. Jiao, B. Zhang, H. Wu, Y. Luo, D. Li, Q. Meng, *Nat. Energy* **2024**, *9*, 1095.
[4] J. Zhou, X. Xu, H. Wu, J. Wang, L. Lou, K. Yin, Y. Gong, J. Shi, Y. Luo, D. Li, H. Xin, Q. Meng, *Nat. Energy* **2023**, *8*, 526.
[5] M. A. Green, E. D. Dunlop, M. Yoshita, N. Kopidakis, K. Bothe, G. Siefer, X. Hao, J. Y. Jiang, *Prog. Photovolt. Res. Appl.* **2025**, *33*, 3.
[6] Y. Gong, Y. Zhang, E. Jedlicka, R. Giridharagopal, J. A. Clark, W. Yan, C. Niu, R. Qiu, J. Jiang, S. Yu, S. Wu, H. W. Hillhouse, D. S. Ginger, W. Huang, H. Xin, *Sci. China Mater.* **2021**, *64*, 52.
[7] Y. Gong, Y. Zhang, Q. Zhu, Y. Zhou, R. Qiu, C. Niu, W. Yan, W. Huang, H. Xin, *Energy Environ. Sci.* **2021**, *14*, 2369.
[8] Y. Gong, Q. Zhu, B. Li, S. Wang, B. Duan, L. Lou, C. Xiang, E. Jedlicka, R. Giridharagopal, Y. Zhou, Q. Dai, W. Yan, S. Chen, Q. Meng, H. Xin, *Nat. Energy* **2022**, *7*, 966.
[9] Y. Gong, A. Jimenez-Arguijo, A. G. Medaille, S. Moser, A. Basak, R. Scaffidi, R. Carron, D. Flandre, B. Vermang, S. Giraldo, H. Xin, A. Perez-Rodriguez, E. Saucedo, *Adv. Funct. Mater.* **2024**, *34*, 2404669.
[10] J. Yang, J. Fu, W. Dong, S. Ren, X. Zhang, J. Su, C. Zhao, M. Wei, D. Zhao, Y. Zhang, S. Wu, Z. Zheng, *Energy Environ. Sci.* **2024**, *17*, 9346.
[11] Y. Zhao, X. Chen, S. Chen, Z. Zheng, Z. Su, H. Ma, X. Zhang, G. Liang, *Adv. Mater.* **2025**, *37*, 2409327.
[12] N.-J. Hao, R.-X. Ding, C.-J. Tong, K. P. McKenna, *J. Appl. Phys.* **2023**, *133*, 145002.
[13] W.-J. Yin, Y. Wu, S.-H. Wei, R. Noufi, M. M. Al-Jassim, Y. Yan, *Adv. Energy Mater.* **2014**, *4*, 1300712.
[14] M. Wong, K. Tse, J. Zhu, *J. Phys. Chem. C* **2018**, *122*, 7759.
[15] J. Wang, J. Shi, K. Yin, F. Meng, S. Wang, L. Lou, J. Zhou, X. Xu, H. Wu, Y. Luo, D. Li, S. Chen, Q. Meng, *Nat. Commun.* **2024**, *15*, 4344.
[16] J. Li, D. B. Mitzi, V. B. Shenoy, *ACS Nano* **2011**, *5*, 8613.
[17] T. Thersleff, S. Giraldo, M. Neuschitzer, P. Pistor, E. Saucedo, K. Leifer, *Mater. Des.* **2017**, *122*, 102.
[18] J. Cong, M. He, J. S. Jang, J. Huang, K. Privat, Y. Chen, J. Li, L. Yang, M. A. Green, J. H. Kim, J. M. Cairney, X. Hao, *Adv. Sci.* **2024**, *11*, 2305938.
[19] M. Ritzer, S. Schönherr, P. Schöppe, W. Wisniewski, S. Giraldo, G. Gurieva, A. Johannes, C. T. Plass, K. Ritter, G. Martínez-Criado, S. Schorr, E. Saucedo, C. Ronning, C. S. Schnohr, *ACS Appl. Energy Mater.* **2020**, *3*, 558.
[20] J. Kim, G. Y. Kim, T. T. T. Nguyen, S. Yoon, Y.-K. Kim, S.-Y. Lee, M. Kim, D.-H. Cho, Y.-D. Chung, J.-H. Lee, M.-J. Seong, W. Jo, *Phys. Chem. Chem. Phys.* **2020**, *22*, 7597.
[21] S. K. Hwang, S. J. Park, J. H. Park, J. H. Yoon, J. Y. Cho, D. K. Cho, J. Heo, G. Y. Kim, J. Y. Kim, *Small* **2024**, *20*, 2307175.
[22] Y. Jian, L. Han, X. Kong, T. Xie, D. Kou, W. Zhou, Z. Zhou, S. Yuan, Y. Meng, Y. Qi, G. Liang, X. Zhang, Z. Zheng, S. Wu, *Small Methods* **2024**, *8*, 2400041.
[23] L. Cao, Z. Zhou, W. Zhou, D. Kou, Y. Meng, S. Yuan, Y. Qi, L. Han, Q. Tian, S. Wu, S. Liu (Frank), *Small* **2024**, *20*, 2304866.
[24] G. Cui, Y. Yang, L. Bai, R. Wang, Z. Gong, Y. Cao, S. Li, X. Lv, C. Zhu, *Small* **2024**, *20*, 2405382.
[25] K. Yin, J. Wang, L. Lou, F. Meng, X. Xu, B. Zhang, M. Jiao, J. Shi, D. Li, H. Wu, Y. Luo, Q. Meng, *Nat. Energy* **2025**, *10*, 205.
[26] Y. Qi, N. Wei, Y. Li, D. Kou, W. Zhou, Z. Zhou, Y. Meng, S. Yuan, L. Han, S. Wu, *Adv. Funct. Mater.* **2024**, *34*, 2308333.
[27] D.-H. Son, H. K. Park, D.-H. Kim, J.-K. Kang, S.-J. Sung, D.-K. Hwang, J. Lee, D.-H. Jeon, Y. Cho, W. Jo, T. Lee, J. Kim, S.-H. Nam, K.-J. Yang, *Carbon Energy* **2024**, *6*, e434.
[28] R. Meng, X. Xu, Y. Huang, L. Wu, J. Li, H. Xu, J. Dong, Y. Liu, X. Fu, H. Guo, G. Wang, Y. Zhang, *Mater. Today Phys.* **2024**, *48*, 101580.
[29] H. Xin, S. M. Vorpahl, A. D. Collord, I. L. Braly, A. R. Uhl, B. W. Krueger, D. S. Ginger, H. W. Hillhouse, *Phys. Chem. Chem. Phys.* **2015**, *17*, 23859.
[30] J. Li, J. Huang, F. Ma, H. Sun, J. Cong, K. Privat, R. F. Webster, S. Cheong, Y. Yao, R. L. Chin, X. Yuan, M. He, K. Sun, H. Li, Y. Mai, Z. Hameiri, N. J. Ekins-Daukes, R. D. Tilley, T. Unold, M. A. Green, X. Hao, *Nat. Energy* **2022**, *7*, 754.
[31] A. Kanevce, M. O. Reese, T. M. Barnes, S. A. Jensen, W. K. Metzger, *J. Appl. Phys.* **2017**, *121*, 214506.
[32] M. F. M. Fathil, M. K. M. Arshad, U. Hashim, A. R. Ruslinda, R. M. Ayub, A. H. Azman, M. Nurfaiz, M. Z. M. Kamarudin, M. Aminuddin, A. R. Munir, Proc. IEEE Int. Conf. Semicond. Electron, Kuala Lumpur, Malaysia, 27-29 August 2014 (IEEE, 2014) **2014**, pp. 24–27.
[33] B. G. Mendis, L. Bowen, Q. Z. Jiang, *Appl. Phys. Lett.* **2010**, *97*, 92112.
[34] J. Quirk, M. Rothmann, W. Li, D. Abou-Ras, K. P. McKenna, *Appl. Phys. Rev.* **2024**, *11*, 11308.
[35] D. Abou-Ras, M. Maiberg, Recombination velocities at grain boundaries in solar-cell absorbers – revisited. *arXiv*. **2025**, DOI: 10.48550/arXiv.2503.08810.
[36] J. Y. W. Seto, *J. Appl. Phys.* **1975**, *46*, 5247.
[37] M. Krause, A. Nikolaeva, M. Maiberg, P. Jackson, D. Hariskos, W. Witte, J. A. Márquez, S. Levcenko, T. Unold, R. Scheer, D. Abou-Ras, *Nat. Commun.* **2020**, *11*, 4189.